Photofission Cross Section and Fissility of Pre-Actinide and Intermediate-Mass Nuclei by 120 - and 145 - MeV Compton Backscattered Photons

M L TERRANOVA

Dipartimento di Scienze e Tecnologie Chimiche, Universita' di Roma "Tor Vergata", and Istituto Nazionale di Fisica Nucleare - INFN, Sezione di Roma 2, 00133 Roma, Italy.

G Ya KEZERASHVILI, A M MILOV, S I MISHNEV, N Yu MUCHNOI, A I NAUMENKOV, I YA PROTOPOPOV, E A SIMONOV and D N SHATILOV

Budker Institute of Nuclear Physics, Russian Academy of Sciences, Siberian Division, 630090 Novosibirsk, Russia.

O A P TAVARES, E DE PAIVA(*) and E L MOREIRA

Conselho Nacional de Desenvolvimento Científico e Tecnológico-CNPq, Centro Brasileiro de Pesquisas Físicas-CBPF, 22290-180 Rio de Janeiro-RJ, Brazil.

Abstract

Cross section measurements for photofission induced in ^{209}Bi, ^{nat}Pb, ^{197}Au, ^{nat}Pt, ^{nat}W, ^{181}Ta, ^{51}V and ^{nat}Ti by 120- and 145-MeV quasi-monochromatic photon beams have been performed at the ROKK-1M facility (BINP, Novosibirsk). The fission yields have been obtained using Makrofol sheets as solid-state fission track detectors. Nuclear fissility values have been deduced on the basis of Levinger's modified quasi-deuteron model of photonuclear interaction, and compared with available literature data. The trend of fissility in the 60-145 MeV energy range has been analysed for various target nuclei as a function of energy and of parameter Z^2/A.

PACS 25.85.-w - Fission reactions.

PACS 25.85.Jg - Photofission.

(*) Fellow, Brazilian CNPq, contract Nr. 840003/92-7

1. Introduction

In recent years high-energy monochromatic photon beams produced by backward scattering of a laser light against high-energy electrons have been widely used for the study of photo-reactions [1]. In particular, a number of photofission cross section and fissility data for actinide, pre-actinide, and intermediate-mass nuclei have been obtained at photon energies $k \leq 100$ MeV with the LADON apparatus at the Frascati National Laboratories [2-7], and at photon energy $k = 100$ MeV with the ROKK-1M facility at the Budker Institute of Nuclear Physics (BINP, Novosibirsk) [8]. Tagged photons produced by the ROKK-2 facility at the storage ring VEPP-3 (BINP) have been recently used for the first time to measure photofissility of ^{209}Bi nucleus in the range 60-270 MeV [9]. Other reliable photofission studies with monochromatic photon beams and/or tagged photons extending over the quasi-deuteron energy region (~ 30-140 MeV) have been reported in refs. [10-18]. All these fissility data have been interpreted successfully on the basis of a two-step model which considers the primary photoabsorption occuring via neutron-proton pairs, followed by a mechanism of fission-evaporation competition for the excited residual nucleus [4, 5, 7, 9, 19]. Although pion photoproduction inside complex nuclei may occur at energies $k \gtrsim 124$ MeV (the pion photoproduction threshold is lowered due to nucleon motion) the contribution of this mechanism to nuclear excitation leading to fission is estimated less than ~30% in the energy range 124-145 MeV.

The present paper reports on the photofission at 120 and 145 MeV of pre-actinide (^{209}Bi, ^{nat}Pb, ^{197}Au, ^{nat}Pt, ^{nat}W, and ^{181}Ta) and intermediate-mass (^{51}V and ^{nat}Ti) nuclei.

Fission of intermediate-mass nuclei means here the break-up of the fissioning system , excited well above the height of the fission barrier (~ 50 MeV [8]), into two fragments of comparable masses. The experiments have been performed taking advantage of the photon doses provided by the ROKK-1M facility and of a method for determination of low fission yields which uses stacks of solid-state nuclear track detectors in contact with thick target metallic samples [20]. The present fission-track-detection technique is suitable for recording fission fragments also in the Ne-Al mass region. On the other hand detection of alpha particles is completely suppressed, as well as that of recoil particles eventually photoproduced from carbon and/or oxigen of the detector material.

Aiming to define the features of photofission in the quasi-deuteron region of photonuclear interaction ($30 \leq k \leq 140$ MeV) , present results and data from previous experiments are discussed , and the variation of fissility for the nuclei under investigation is analysed as a function of energy k and of parameter Z^2/A.

2 . Experimental

The experiments were done following the arrangement and methodology described in details in our previous work [8]. The stacks of the various target and detector materials (metallic foils and makrofol polycarbonate sheets) were exposed perpendicularly to monochromatic photon beams produced at the ROKK-1M facility by Compton backscattering of laser light (2.34 or 2.41 eV) against high-energy (2.0 or 2.2 GeV) electrons circulating in the VEPP-4M storage ring. The experimental arrangement is shown in fig.1 .The energy spectra were taken by a NaI(Tl) total photo-

absorption calorimeter, and typical spectra are presented in fig. 2 for the 134 MeV and 165 MeV Compton-edge (k_{max}) energy values. Coincidences between the signals coming from the NaI(Tl) calorimeter, scintillation counter and laser pulses have been used to define the contributions of Compton, bremsstrahlung, and charged particles components in the flux (details can be seen in refs. [8, 21]). The bremsstrahlung impurity in the photon beams was estimated in 5%, and the percentage of charged particles in the total dose amounted to less than 1% (k_{max} = 134 MeV) and 9% (k_{max} = 165 MeV). Information concerning the target and detector materials (nature, physical characteristics, composition of the stacks, type of detector) as well as the irradiation conditions (beam intensity, resolution, total photon dose) for the two exposures performed at BINP (Novosibirsk) has been summarized in table 1.

After irradiation, the detector foils were processed by the usual etching procedure in order to produce legible etched fission tracks on the detector surface for track couting by conventional optical microscopy (table 2). In view of the large number of detectors to be analyzed (a total of 405 in two runs) , track identification and counting on each detector was done by one observer (single scanning) and checked by a second one. A counting efficiency of (79 ± 7)% has been considered for fission track loss during track analysis, as in previous measurements with the same scanning methodology [4-7]. Besides, for each stack of a given target element, the mapping of all fission tracks recorded was constructed from their coordinate positions to define the final number of fission tracks (4^{th} and 9^{th} columns in table 2).

3. Photofission yield, absolute cross section and fissility

Besides statistics and efficiency of fission track counting, and appropriate correction for gamma-beam attenuation through the stacks (tables 1 and 2), it is essential to consider also the effect of self-absorption of fission fragments by the target materials (thin- and thick-target geometry) to determine correctly the photofission yield. This latter effect allows one to obtain the effective target thickness, x, of each target material, and also the average total efficiency , ε, of the detection method (etching efficiency multiplied by observation efficiency). A method for evaluating the values of these two quantities has been reported elsewhere [6, 20], and it takes into account i) the average residual range of the full-energy median fission fragment in both target and detector materials, ii) the thickness of the surface layer of the detector removed by etching, and iii) the minimal etched fission track projection capable of being observed on the detector surface under given optics. Accordingly, for fission experiments in which thin or thick target meterials are used in close contact with fission-track detectors, the fission yield is given by

$$Y = C \frac{N_T}{Q \sum_i n_i \varepsilon_i x_i}, \qquad (1)$$

where $C = M / (\rho N_0)$ is a constant for each target element, M is the atomic weight (in g) , ρ is the density (in g cm^{-3}) , N_0 is Avogadro's number, and the other quantities appearing in eq. (1) are defined in tables 1-3. For each target element the values of Q are listed in table 1, N_T and n_i ($i = 1, 2$) in table 2 , and C, ε_i , and x_i, in table 3. The last

two columns in table 3 report the final values of the photofission yield obtained at k_{max} = 134 MeV and k_{max} = 165 MeV for the various target nuclei. It is seen that the measured photofission yields are indeed very low (order of units or tens of μb). The total uncertainties associated with the yield-values have been estimated by considering both statistical and systematic errors. The latter ones mainly come from the incertainties related to the determination of effective target thickness and total detection efficiency . Systematic errors amount to ~13-16% for Pt, W, Ta, V, and Ti targets , and ~18-23 % for Pb and Au targets. The statistical errors have been evaluated as follows: 21-25% for Pb, Pt, W, Ta, and Ti targets, 60% for Au, and 30% for V in the case of k_{max} = 134 MeV ; 20-22% for Pb and W targets, 17% for Pt, 26-28% for Ta, Au, and Ti, and 36% for V in the case of k_{max} = 165 MeV . For Bi targets, in both irradiations the statistical error was estimated ~ 18% , while the systematic error amounted to ~ 24%

The physical quantity of interest, however, is the absolute photofission cross section, σ_f. This quantity is related to photofission yield , Y, by means of

$$Y = \int_{k_i}^{k_f} \sigma_f(k) \left(\frac{dn}{dk}\right) dk, \qquad (2)$$

where k_i and k_f are the limiting energy values in the photon spectrum, and dn/dk is the photon energy distribution normalized to one photon in the interval k_i - k_f (fig. 2). The product $\sigma_f(k) \cdot (dn/dk) = s(k)$ represents the fission-yield strength at photon energy k. For pre-actinide target nuclei the relative contributions to total fission yield due to low - ($k << k_{max}$) and high-energy ($k > k_{max}$) photons in the spectrum can be evaluated by rewriting eq. (2) as

(3) $$Y = \int_{k_{th}}^{k_1} s(k)dk + \int_{k_1}^{k_2} s(k)dk + \int_{k_2}^{k_f} s(k)dk,$$

where $k_{th} > k_1$ represents the photofission energy threshold, i.e., the lowest photon energy for which fission can be detected, in such a way that $\int_{k_1}^{k_{th}} s(k)dk = 0$. The interval k_1 - k_2 contains the peak-shape of the energy distribution . Such interval is defined by the condition

(4) $$\int_{k_{th}}^{k_1} s(k)dk + \int_{k_2}^{k_f} s(k)dk << \int_{k_{th}}^{k_f} s(k)dk,$$

where it is reasonable to assume that 20-25% of fission events are produced by low- and high-energy photons, in view of the errors affecting the experimental fission yields and of the energy resolution of the photon beams (20-24%). Finally, since the peak shape of the spectrum is reasonably narrow in the range k_1 - k_2, we can write $\sigma_f(\bar{k}) = \alpha Y$, where $\bar{k}$ is the effective photon mean energy calculated in the interval k_1 - k_2, and α is a numerical factor. Both $\bar{k}$- and α-values are found to vary not significantly for all pre-actinide nuclei. Figure 3 shows, for example, the behavior of fission-yield strength which is obtained for Bi, Pb, and Au targets irradiated at 165-MeV Compton-edge energy. In this case, the following values are found: $\bar{k}$ = 145 MeV and α = 1.43. The same procedure has been applied to the irradiation of k_{max} = 134 MeV, thus obtaining $\bar{k}$ = 120 MeV and α = 1.45.

For ^{51}V and ^{nat}Ti target nuclei the lowest photon energy for which fission can be detected has been estimated as $k_{th} \approx$ 50 MeV [8], and the trend of $\sigma_f(k)$ is unknown.

In this case, the best we can do is to retain for these two nuclei the same values of $\bar{k}$ as calculated for the pre-actinide nuclei, and write

$$(5) \qquad \sigma_f(\bar{k}) = \alpha' Y, \qquad \alpha' = \left[\int_{k_1}^{k_f} \left(\frac{dn}{dk} \right) dk \right]^{-1},$$

where $\bar{k}$ is now defined in the range k_1 - k_f. In this way one obtained $\alpha' = 1.59$ for $k_{max} = 134$ MeV, and $\alpha' = 1.60$ for $k_{max} = 165$ MeV. The resulting absolute photofission cross-section-values ($\sigma_f(\bar{k}) = \alpha Y$ or $\sigma_f(\bar{k}) = \alpha' Y$) are reported in table 4 for $\bar{k}$ = 120 and 145 MeV (respectively, in the 3rd and 6th columns). The uncertainty associated with the α - and α'-values amounts to 1-2%, therefore one may consider it negligible if compared with the total error affecting the yield-values.

Photofissility values at each mean incident photon energy for the target nuclei under investigation have been deduced by calculating the ratio

$$(6) \qquad f = \frac{\sigma_f}{\sigma_a^{\cdot}}.$$

Here, the values of total nuclear photoabsorption cross section , $\sigma_a^{\cdot}$, have been calculated by the usual parameterization following Levinger's modified quasi-deuteron model [27] , as detailed in [8]. Fissility as defined in equation (6) represents the product of the probability of formation of a residual nucleus times the total fission probability for this residual, summed over all the possible modes of obtaining excited residual nuclei after absorption of the incoming photon [9, 19] . The values obtained for both quantities $\sigma_a^{\cdot}$ and f are listed in table 4.

4. Discussion and conclusion

Photofissility values have been plotted *vs* incident photon energy in the quasi-deuteron region of photonuclear absorption (figs. 4 and 5). In these figures filled circles represent the data of the present work , open squares represent the data of our previous work at the ROKK-1M facility [8] , whereas open circles are data obtained with the LADON beam at Frascati [4, 6]. For comparison, we chose to represent in fig.5 the fissility data for ^{174}Yb and ^{154}Sm (open triangles), which data were deduced from the photofission cross section values resulting from the unfolding of the electrofission yields with a virtual photon spectrum [23]. Inspection of figs. 4 and 5 shows a general trend of increasing fissility with increasing photon energy for both pre-actinide and intermediate-mass nuclei. This behavior is consistent with that inferred from early photofission data taken with bremsstrahlung radiation as a source of real photons incident on Bi, Pb, Tl, Au, Pt, Os, Re, Ta, and Hf target nuclei [25, 28]. Moreover, apart from a few data-points, the present data are also consistent with the general rule that fissility varies exponentially with both Z^2/A and excitation energy ($E^* \approx k$). This is better evidenced in fig. 6, where fissility data show to increase with Z^2/A for nuclei of mass number $A > 150$. Assuming for simplicity a linear dependence of log f with Z^2/A in the range $28 < Z^2/A < 33$, a least-squares treatment of the data of fig. 6 gives for the ratio of fissility at the higher energies and 100 MeV incident photons

$$(7) \qquad \log \frac{f(120)}{f(100)} = 0.08317\left[33.17 - Z^2/A\right]; \log \frac{f(145)}{f(100)} = 0.07450\left[35.64 - Z^2/A\right].$$

These ratios not only indicate an increase of fissility with increasing incident energy, but also that this behaviour is more pronounced as we go towards less massive pre-actinide nuclei (as an example, for ^{174}Yb we have f(120) /f(100) = 2.6 and f(145) /f(100) = 3.6 , while for ^{209}Bi the ratios are 1.04 and 1.6, respectively). This result is consistent with the predictions based on the fission-evaporation competition model by Nix and Sassi [29] as well as with the cascade-evaporation calculation model by Iljinov *et al.* [30].

Concerning ^{51}V and ^{nat}Ti target nuclei, the fissility data of the present work (table 4 and fig. 6) seem to confirm the increasing of fissility for fissioning systems of $Z^2/A \leq 20$ already found at lower energies [7, 8]. Overall our data are consistent with the predictions from the current models [29, 30] which have indicated a clear trend of increasing fissility with decreasing Z^2/A in the region of nuclei less massive than silver. We remark that this is the first set of fissility data available up to now for nuclei of $A \approx 50$ in the quasi-deuteron region of photonuclear absorption. A detailed semiempirical treatment of these data , based on the current, two-step model for photofission reactions [9, 19] is clearly needed in order to better describe the features of nuclear fissility . This will be the subject of future work.

* * * * * * * * * *

The authors are thankful to the management of the Budker Institute of Nuclear Physics - BINP (Novosibirsk) for supporting the present research. Thanks are due to the experimental staff of the storage ring VEPP-4M and to the technical group of the ROKK-1M facility for providing high-quality photon beams. It is a pleasure to acknowledge valuable suggestions by Prof. C. Schaerf. Partial support by the Italian INFN (sezione di Roma 2) and the Brazilian CNPq is also gratefully acknowledged.

References

[1] Babusci D , Bellini V ,Capogni M ,Casano L, D'Angelo A, Ghio F , Girolami B, Hu L, Moricciani D and Schaerf C 1996 *Riv. Nuovo Cimento* **19** (N.5).

[2] Bernabei R, De Oliveira V C, Martins J B, Tavares O A P , Pinheiro Filho J D, D'Angelo S , De Pascale M P , Schaerf C and Girolami B 1988 *Nuovo Cimento A* **100** 131.

[3] Martins J B , Moreira E L, Tavares O A P, Vieira J L, Pinheiro Filho J D, Bernabei R, D'Angelo S , De Pascale M P , Schaerf C. and Girolami B 1989 *Nuovo Cimento A* **101** 789.

[4] Martins J B, Moreira E L, Tavares O A P, Vieira J L, Casano L , D'Angelo A, Schaerf C , Terranova M L , Babusci D and Girolami B 1991 *Phys. Rev. C* **44** 354.

[5] Tavares O A P , Terranova M L , Casano L , D'Angelo A, Moricciani D, Schaerf C , Babusci D , Girolami B , Martins J B , Moreira E L and Vieira J L 1991 *Phys. Rev. C* **44** 1683.

[6] Tavares O A P, Martins J B , De Paiva E , Moreira E L , Vieira J L , Terranova M L , Capogni M , Casano L , D'Angelo A , Moricciani D , Ghio F , Girolami B and Babusci D 1993 *J. Phys. G: Nucl. Part. Phys.* **19** 805.

[7] Tavares O A P , Martins J B , Moreira E L , Terranova M L , Capogni M , Casano L , D'Angelo A , Moricciani D , Schaerf C , Girolami B , Ghio F and Babusci D 1993 *J. Phys. G: Nucl. Part. Phys.* **19** 2145.

[8] Terranova M L , Tavares O A P, Kezerashvili G Ya , Kiselev V A , Milov A M , Muchnoi N Yu , Naumenkov A I , Petrov V V, Protopopov I Ya , Simonov E A , De Paiva E and Moreira E L 1996 *J. Phys. G: Nucl. Part. Phys.* **22** 511.

[9] Terranova M L, Kezerashvili G Ya , Kiselev V A , Milov A M , Mishnev S I , Protopopov I Ya , Rotaev V N , Shatilov D N and Tavares O A P 1996 *J. Phys. G: Nucl. Part. Phys.* **22** 1661.

[10] Lemke H -D , Ziegler B , Mutterer M , Theobald J P and Cârjan N 1980 *Nucl. Phys. A* **342** 37.

[11] Bellini V , Emma V , Lo Nigro S , Milone C , Pappalardo G S , De Sanctis E, Di Giacomo P, Guaraldo C , Lucherini V , Polli E and Reolon A R. 1983 *Nuovo Cimento Lett* **36** 587.

[12] Guaraldo C , Lucherini V , De Sanctis E , Levi Sandri P , Polli E , Reolon A R , Lo Nigro S , Aiello S , Bellini V , Emma V , Milone C and Pappalardo G S 1987 *Phys. Rev. C* **36** 1027.

[13] Lucherini V , Guaraldo C , De Sanctis E , Levi Sandri P , Polli E , Reolon A R Iljinov A S , Lo Nigro S , Aiello S , Bellini V , Emma V , Milone C , Pappalardo G S and Mebel M V 1989 *Phys. Rev. C* **39** 911.

[14] Iljinov A S , Ivanov D I , Mebel M V , Nedorezov V G , Sudov A S and Kezerashvili G Ya 1992 *Nucl. Phys. A* **539** 263.

[15] Ivanov D I, Kezerashvili G Ya , L'Vov A I , Mishnev S I , Nedorezov V G , Protopopov I Ya and Sudov A S 1992 *Yad. Fiz.* **55** 3 [1992 *Sov. J. Nucl. Phys* **55** 1].

[16] Leprêtre A , Bergère R, Bourgeois P , Carlos P , Fagot J , Fallou J L, Garganne P, Veyssière A , Ries H , Göbel R , Kneissl U , Mank G, Ströher H , Wilke W, Ryckbosch D and Jury J 1987 *Nucl. Phys. A* **472** 533.

[17] Ahrens J , Arends J , Bourgeois P , Carlos P , Fallou J L , Floss N , Garganne P, Huthmacher S , Kneissl U , Mank G , Mecking B , Ries H , Stenz R and Veyssière A 1984 *Phys. Lett. B* **146** 303.

[18] Bellini V , Emma V , Lo Nigro S , Milone C , Pappalardo G S , De Sanctis E , Di Giacomo P , Guaraldo C , Lucherini V , Polli E and Reolon A R 1985 *Nuovo Cimento A* **85** 75.

[19] Tavares O A P and Terranova M L 1992 *Z. Phys. A - Hadrons and Nuclei* **343** 407.

[20] Tavares O A P 1991 *Radiat. Effects Defects Solids* **118** 105.

[21] Kezerashvili G Ya , Milov A , Muchnoi N Yu and Usov A 1993 *Proc. XIII Panic (Perugia)* vol. II p. 839 ; Kezerashvili G Ya *et al* 1995 ., *High Energy Spin Physics, Proc. XI Int. Symp. (Bloomington)* vol. 343 (Heller K J and Smith S L Editors Woodbury, NY: AIP) p. 260.

[22] Warnock R V and Jensen R C 1968 *J. inorg. nucl. Chem* **30** 2011.

[23] Moretto L G , Gatti R C , Thompson S G , Routti J T , Heisenberg J H, Middleman L M , Yearian M R and Hofstadter R 1969 *Phys. Rev.* **179** 1176.

[24] Arruda-Neto J D T , Sugawara M , Tamae T , Sasaki O, Ogino H , Miyase H and Abe K 1986 *Phys. Rev. C* **34** 935.

[25] Ranyuk Yu N and Sorokin P V 1967 *J. Nucl. Phys. (USSR)* **5** 37 [1967 *Sov. J. Nucl. Phys.* **5** 26].

[26] Arruda-Neto J D T , Sugawara M , Miyase H , Kobayashi T , Tamae T , Abe K , Nomura M, Matsuyama H, Kawahara H, Namai K, Yoneama M L and Simionatto S 1990 *Phys. Rev. C* **41** 354.

[27] Levinger J S 1979 *Phys. Lett. B* **82** 181.

[28] Minarik E V and Novikov V A 1957 *J. Exptl. Theoret. Phys. (USSR)* **32** 241 [1957 *Sov. Phys. JETP* **5** 253].

[29] Nix J R and Sassi E 1966 *Nucl. Phys.* **81** 61.

[30] Iljinov A S , Cherepanov E A and Chigrinov S E 1980 *Yad. Fiz* **32** 322 [1980 *Sov. J. Nucl. Phys.* **32** 166].

Table 1 - *Data regarding the targets, detectors, and irradiation conditions*

Target material(a)		Irradiation conditions					
Element	Nominal thickness x_0 (μm)	134-MeV Compton-edge energy(d)			165-MeV Compton-edge energy(e)		
		Nr. of targets	Nr.(type) of detectors(f)	Nominal, total photon dose(g) $Q(10^8\ \gamma)$	Nr. of targets	Nr.(type) of detectors(f)	Nominal, total photon dose(g) $Q(10^8\ \gamma)$
Bi	5.2±1.0(b)	8	8(2)	38.3	16	8(1)+8(2)	32.1
Pb	3.1±0.4(b)	8	8(2)	38.5	16	8(1)+8(2)	32.4
Au	0.70±0.12(b)	8	8(2)	38.6	16	8(1)+8(2)	32.4
Pt	26(c)	19	38(2)	40.9	19	18(1)+20(2)	34.7
W	50(c)	25	50(2)	48.8	25	25(1)+25(2)	41.3
Ta	26(c)	24	48(2)	59.0	24	23(1)+25(2)	49.9
	50(c)	6	12(2)		6	6(1)+6(2)	
V	15(c)	6	12(2)	63.7	6	12(1)	54.1
Ti	24(c)	7	14(2)	64.1	7	14(1)	54.4

(a) All targets of natural isotopic composition.
(b) Average value over 24 high-purity metal films prepared by vacuum evaporation on 3.5 cm x 3.5 cm foils of 1.72mg.cm^{-2} thick Mylar as supports.
(c) High-purity metallic foils.
(d) Photon beam intensity: up to $2 \cdot 10^6\ \gamma\ s^{-1}$; resolution ($FWHM/k_{max}$): 20% (see fig.2).
(e) Intensity: up to $3 \cdot 10^6\ \gamma\ s^{-1}$; resolution: 24% (see fig.2).
(f) These are 100-μm (type 1) or 145-μm (type 2) thick sheets of Makrofol N polycarbonate fission-track detectors supplied by Bayer AG (Germany).
(g) Attenuation of the photon dose throughout the stacks estimated by the law of exponential decrease of photon beam intensity.

CBPF-NF-055/97

Table 2 - *Data regarding the processing and analysis of detectors*[a]

Target nucleus	Photon beam of 134-MeV Compton-edge			Photon beam of 165-MeV Compton-edge				
	Amount of etching[b]	Nr. of detectors analysed[c]	Nr. of fission tracks recorded[d]	Amount of etching[b]		Nr. of detectors analysed[c]		Nr. of fission tracks recorded[d]
	h_2(μm)	n_2	N_T	h_1(μm)	h_2(μm)	n_1	n_2	N_T
Bi	0.53 ± 0.06	8	42 ± 8	0.73 ± 0.04	0.53 ± 0.06	8	1	59 ± 10
Pb	idem	8	30 ± 7	idem	idem	8	1	39 ± 8
Au	idem	8	5 ± 3	idem	idem	8	7	14 ± 4
Pt	idem	38	30 ± 7	idem	idem	18	20	52 ± 9
W	idem	50	38 ± 8	idem	idem	25	25	27 ± 6
Ta	idem	60	30 ± 7	idem	idem	29	31	19 ± 5
V	0.88±0.10	12	14 ±4	1.09 ± 0.06	0.79 ± 0.09	12	0	11 ± 4
Ti	0.79±0.09	14	20 ± 5	idem	idem	14	0	15 ± 4

(a) Subscripts for the different quantities indicate the type of detector used (see footnote f in table 1).
(b) Etching conditions: 6.25-N NaOH solution, 60° C, gentle stirring; *h* is the thickness of detector layer removed by etching.
(c) Leitz Ortholux microscopes (objectives 25x or 45x, oculars 12.5x or 10x).
(d) Corrected for a counting efficiency of 0.79 ±0.07; statistical error indicated.

CBPF-NF-055/97

Table 3 - *Data regarding the determination of photofission yield*[a]

Target nuleus	C ($10^{-11}\mu m^3$)	Target effective thickness[b] (μm)		Detection efficiency[b] (%)		Photofission yield[c], Y(mb)	
		x_1	x_2	ε_1	ε_2	k_{max}=134 MeV	k_{max} =165 MeV
Bi	3.56	3.8	3.9	87	88	0.14±0.04	0.22±0.06
Pb	3.03	3.1	3.2	72	72	0.13±0.04	0.18±0.05
Au	1.69	0.7	0.7	93	95	$(41\pm26)\cdot10^{-3}$	$(74\pm27)\cdot10^{-3}$
Pt	1.51	3.0	3.0	48	50	$(19\pm5)\cdot10^{-3}$	$(40\pm9)\cdot10^{-3}$
W	1.58	3.1	3.1	47	49	$(16\pm4)\cdot10^{-3}$	$(14\pm4)\cdot10^{-3}$
Ta	1.80	3.5	3.5	47	49	$(9.0\pm 2.5)\cdot10^{-3}$	$(6.8\pm2.1)\cdot10^{-3}$
V	1.38	2.5	2.4	19	22	$(48\pm16)\cdot10^{-3}$	$(49\pm18)\cdot10^{-3}$
Ti	1.75	3.1	3.0	15	20	$(65\pm20)\cdot10^{-3}$	$(74\pm22)\cdot10^{-3}$

(a) Yields are given by eq. (1).
(b) Subscripts indicate the type of detector used (see footnote f in table 1).
(c) Statistical plus systematic errors included.

CBPF-NF-055/97

Table 4 - *Photofission (σ_f) and total nuclear photoabsorption (σ'_a) cross section data and fissility ($f=\sigma_f/\sigma'_a$) at 120- and 145-MeV effective photon mean energy ($\bar{k}$)*

Target nucleus(a)	Z^2/A	$\bar{k}$=120 MeV			$\bar{k}$=145 MeV		
		σ_t(mb)	σ_a'(mb)	f	σ_t(mb)	σ_a'(mb)	f
^{209}Bi	32.96	0.20±0.06	12.8±1.7	$(1.6\pm0.5)\cdot10^{-2}$	0.31±0.08	12.5±1.6	$(2.5\pm0.7)\cdot10^{-2}$
^{207,2}Pb	32.45	0.19±0.06	12.7±1.6	$(1.5\pm0.5)\cdot10^{-2}$	0.26±0.07	12.4±1.5	$(2.1\pm0.6)\cdot10^{-2}$
^{197}Au	31.68	$(59\pm38)\cdot10^{-3}$	12.3±1.6	$(4.8\pm3.1)\cdot10^{-3}$	$(11\pm4)\cdot10^{-2}$	12.0±1.5	$(9.2\pm3.5)\cdot10^{-3}$
^{195,1}Pt	31.18	$(27\pm7)\cdot10^{-3}$	12.2±1.6	$(2.2\pm0.6)\cdot10^{-3}$	$(57\pm13)\cdot10^{-3}$	11.9±1.5	$(4.8\pm1.2)\cdot10^{-3}$
^{183,9}W	29.78	$(23\pm6)\cdot10^{-3}$	11.7±1.5	$(2.0\pm0.6)\cdot10^{-3}$	$(20\pm6)\cdot10^{-3}$	11.4±1.4	$(1.7\pm0.6)\cdot10^{-3}$
^{181}Ta	29.44	$(13\pm4)\cdot10^{-3}$	11.6±1.5	$(1.1\pm0.4)\cdot10^{-3}$	$(9.7\pm3.0)\cdot10^{-3}$	11.3±1.4	$(8.6\pm2.8)\cdot10^{-4}$
^{51}V	10.37	$(76\pm25)\cdot10^{-3}$	4.1±1.2	$(1.8\pm0.8)\cdot10^{-2}$	$(78\pm29)\cdot10^{-3}$	3.8±1.1	$(2.0\pm1.0)\cdot10^{-2}$
^{47,9}Ti	10.10	$(10\pm3)\cdot10^{-2}$	3.8±1.1	$(2.6\pm1.1)\cdot10^{-2}$	$(12\pm3)\cdot10^{-2}$	3.6±1.0	$(3.3\pm1.2)\cdot10^{-2}$

(a) Mean mass number of the naturally occurring isotopes.

CBPF-NF-055/97

FIGURE CAPTIONS

Fig.1 - Experimental set-up of the ROKK-1M facility at the storage ring VEPP-4M (BINP, Novosibirsk, Russia). L1 is a focusing lens ; M1, M2 are mirrors; C is a 4 mm x 4 mm collimatpr of 10 cm of lead ; CM is a cleaning magnet ; SC is a scintillation counter ; T + D are the stacks of targets and makrofol detectors ; PC is a proportional chamber with 2 mm lead converter ; NaI(Tl) is a total photoabsorption calorimeter of 10 cm x 10 cm x 40 cm for gamma-beam spectrometry and dose measurements.

Fig.2-Typical spectra of backscattered Compton γ-beams (normalized to one photon) taken with the NaI(Tl) calorimeter after collimation. Curve 1: $k_{max} = 134$ MeV, $\bar{k} = 120$ MeV ; curve 2 : $k_{max} = 165$ MeV, $\bar{k} = 145$ MeV .

Fig.3- (a) Fission-yield strength, $\sigma_f(k) \cdot (dn/dk)$, plotted against photon energy for Bi target at 165-MeV Compton-edge energy. $\sigma_f(k)$ is the average photofission cross section trend from data of [4, 10-12, 22-24], and dn/dk is the measured Compton spectrum shown in fig.2 (curve 2). The energy values k_{th}, , k_1 ,k_2 , and k_f define the various energy regions in eq.(3). The same is shown for Pb (b) and Au (c) targets: $\sigma_f(k)$ is the average trend from data of [13, 25] for Au, and the measured σ_f-curve of [26] for Pb.

Fig.4.- Variation of nuclear fissility, f, with photon energy , k , for Bi, Pb, Au, Pt , and W targets . data points represent f-values obtained with Compton backscattered photon beams : ○, LADON beam at Frascati [4,6] ; □ , ROKK-1M beams at Novosibirsk [8] : ●, ROKK-1M beams at Novosibirsk (this work) . The dashed curves are to guide the eyes.

Fig.5- The same as in fig.4 for Ta, V, and Ti targets. Also shown are the data for ^{174}Yb and ^{154}Sm (Δ) obtained with virtual photons [23] .

Fig.6- Nuclear fissility plotted against parameter Z^2/A of the target nucleus. Data of the present measurements at 120- and 145-MeV incident photons are reported, respectively, in b) and c) ; previous data at 100-MeV incident photons [8] are reproduced in a) . Points are experimental data : ● , ^{209}Bi, , ^{nat}Pb, ^{197}Au, ^{nat}Pt, ^{nat}W, ^{181}Ta, ^{51}V, and ^{nat}Ti of this work and [8] ; ○ , ^{209}Bi of [12] ; ▽ , ^{nat}Tl of [28] ; Δ , ^{174}Yb of [23] ; □ , ^{209}Bi of [25] ; ⊠ , ^{197}Au of [13]; ◇ , ^{209}Bi of [11]. The full lines are least-squares fits of the data in the range $28< Z^2/A <33$. To facilitate a comparison between the present results and the 100-MeV data, the full line in a) is reproduced (dashed line) also in b) and c) .

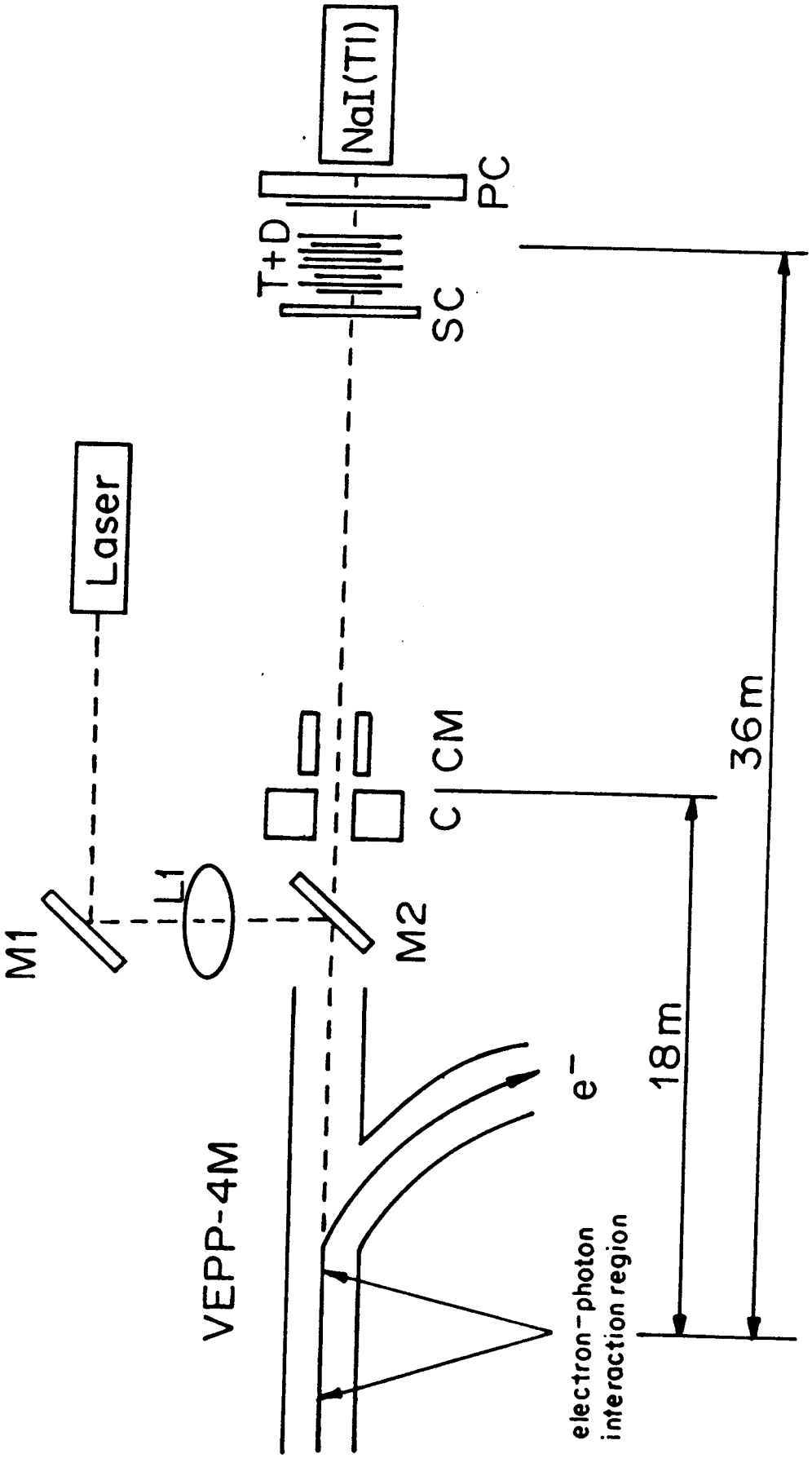
NaI(Tl)
PC
T+D
SC
Laser
CI CM
36m
L1
M1
M2
18m
e⁻
VEPP-4M
electron-photon
interaction region

Fig. 1

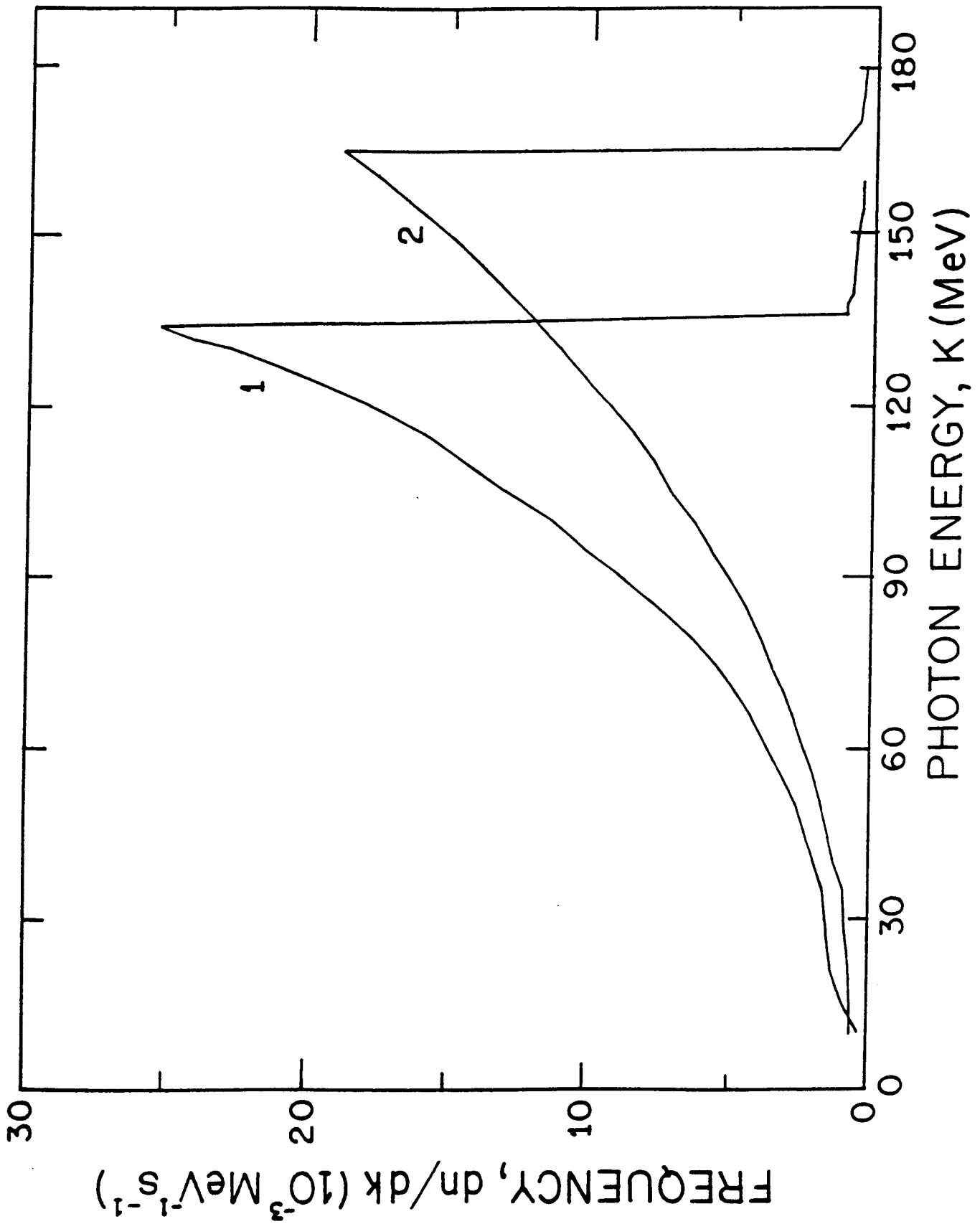
FREQUENCY, dn/dk (10^{-3} MeV^{-1}s^{-1})
0
10
20
30
PHOTON ENERGY, K (MeV)
0
30
60
90
120
150
180
1
2

Fig. 2

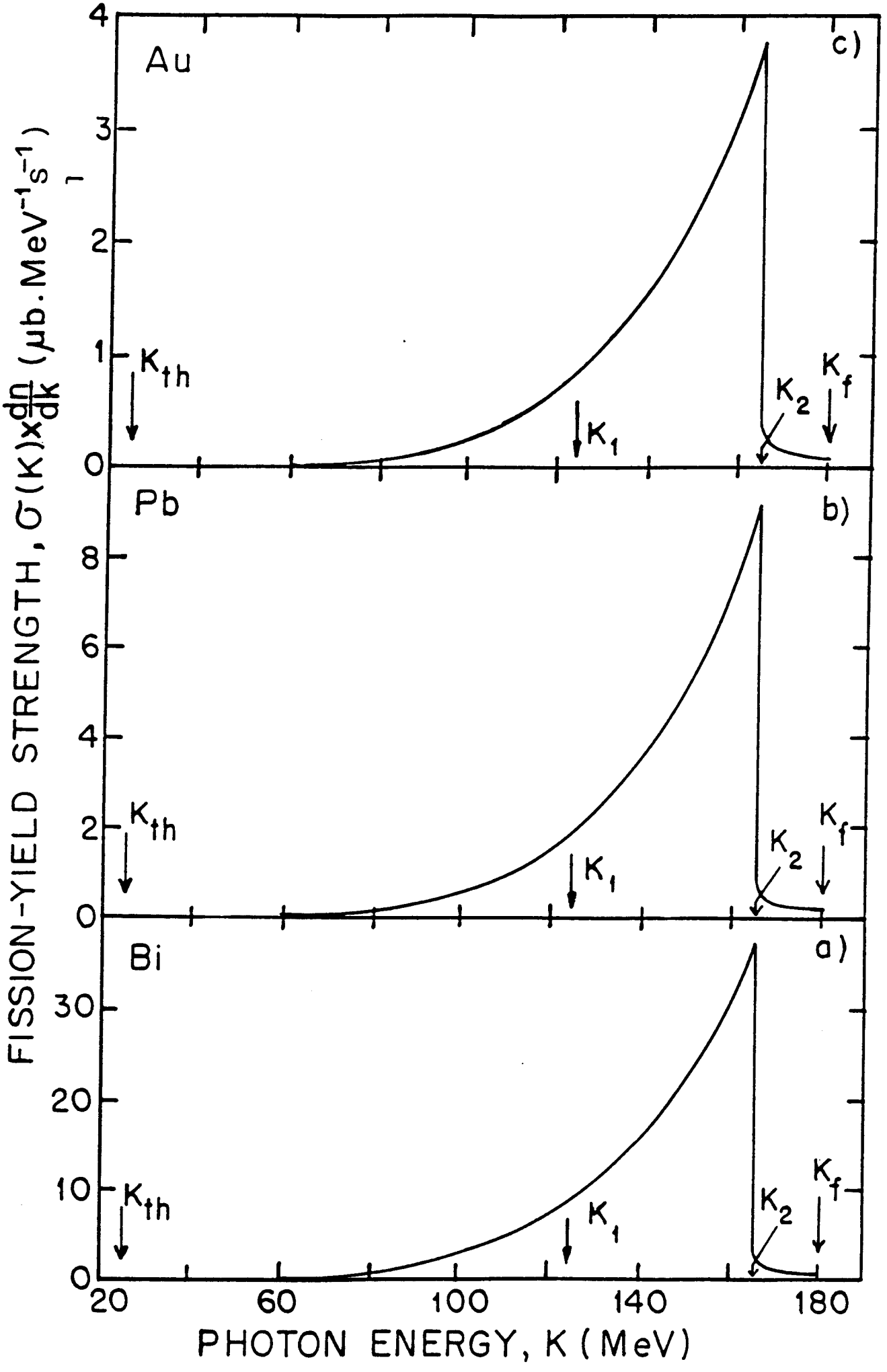
Au
c)
Pb
b)
Bi
a)
K_{th}
K_1
K_2
K_f
FISSION-YIELD STRENGTH, $\sigma(K)x\frac{dn}{dk}$ ($\mu b.MeV^{-1}s^{-1}$)
PHOTON ENERGY, K (MeV)
0
1
2
3
4
0
2
4
6
8
0
10
20
30
20
60
100
140
180

Fig. 3

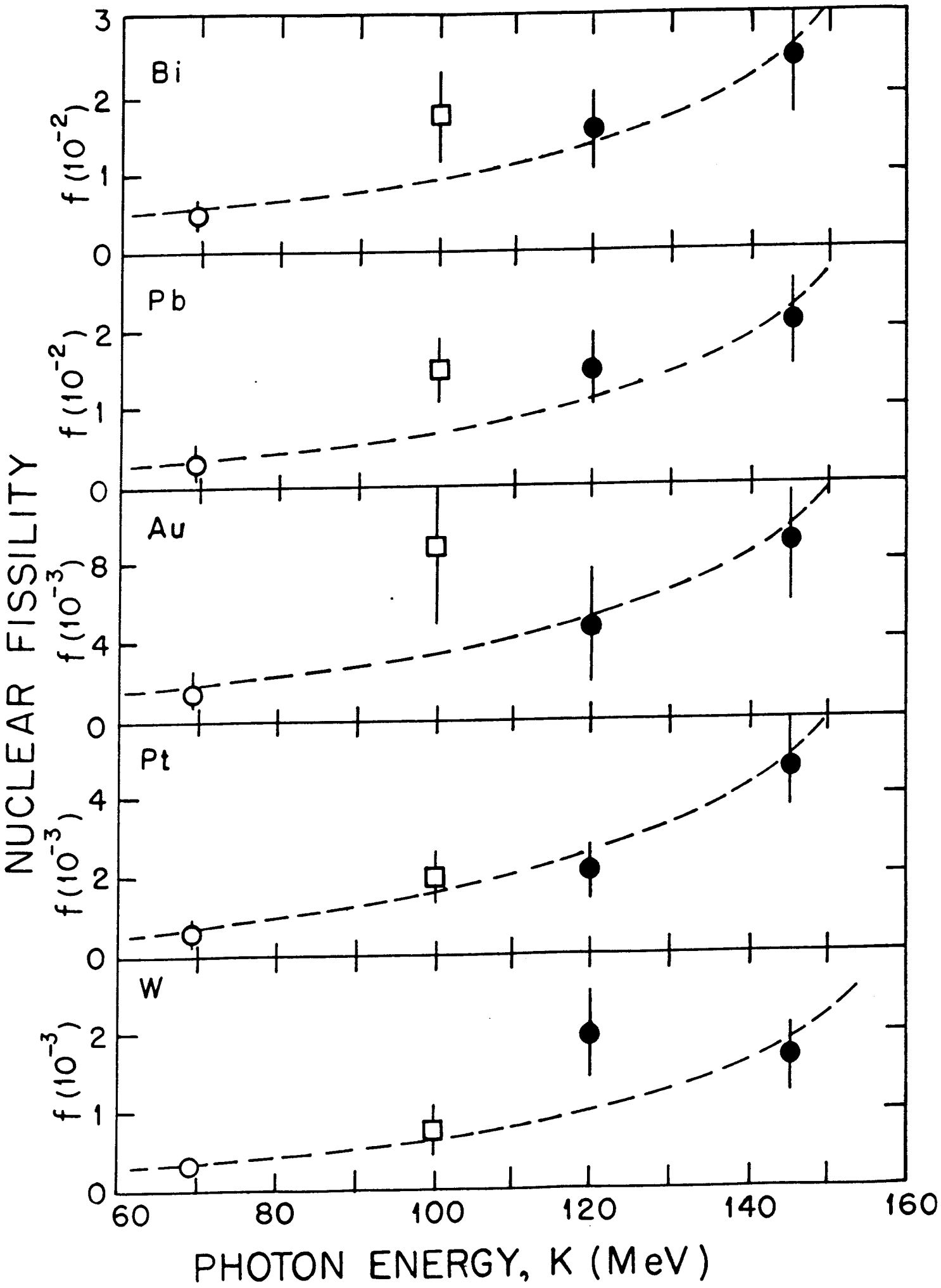
NUCLEAR FISSILITY
Bi
Pb
Au
Pt
W
f (10^-2)
f (10^-3)
0
1
2
3
4
8
60
80
100
120
140
160
PHOTON ENERGY, K (MeV)

Fig. 4

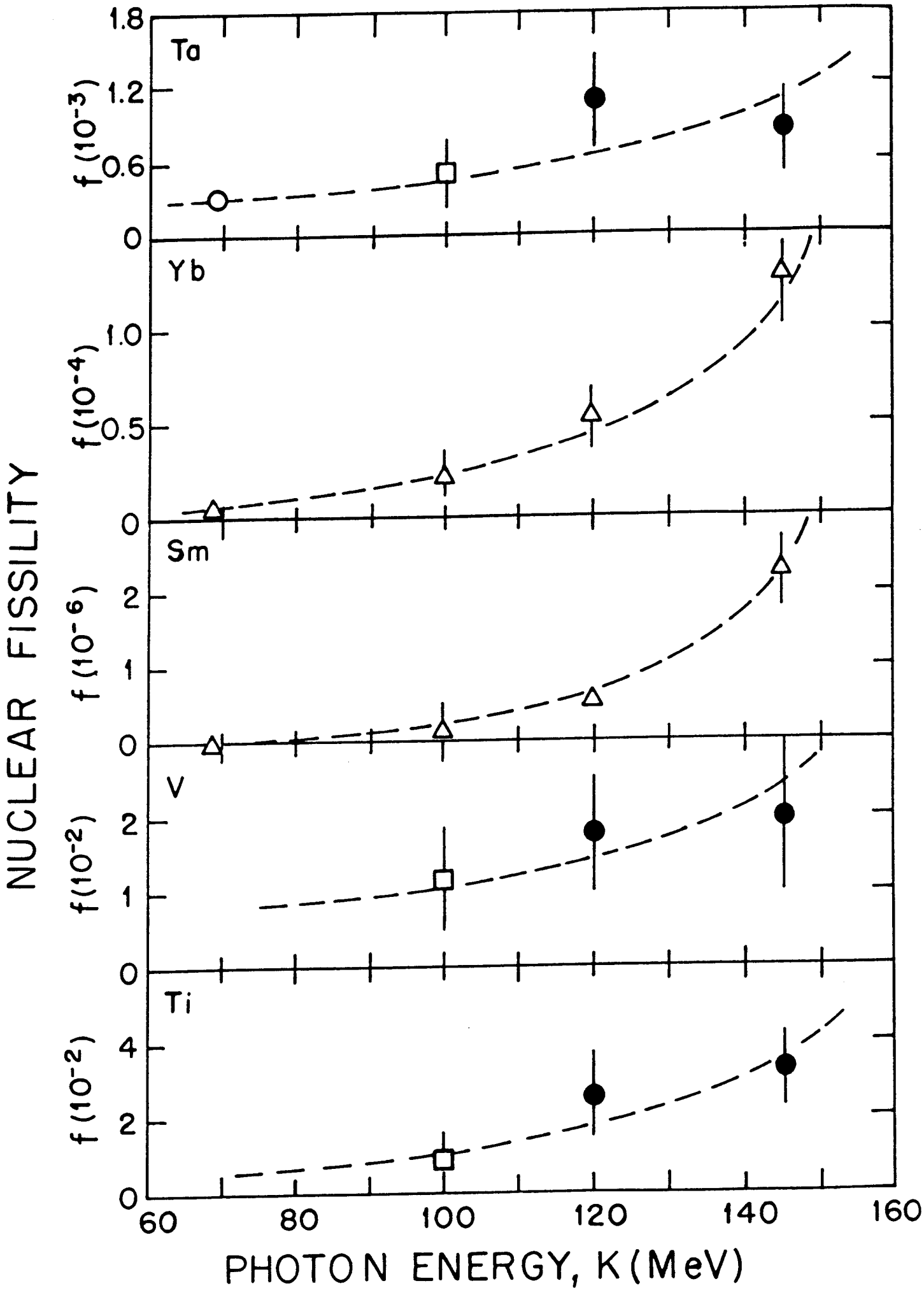
NUCLEAR FISSILITY
Ta
f (10⁻³)
1.8
1.2
0.6
0
Yb
f (10⁻⁴)
1.0
0.5
0
Sm
f (10⁻⁶)
2
1
0
V
f (10⁻²)
2
1
0
Ti
f (10⁻²)
4
2
0
60
80
100
120
140
160
PHOTON ENERGY, K (MeV)

Fig. 5

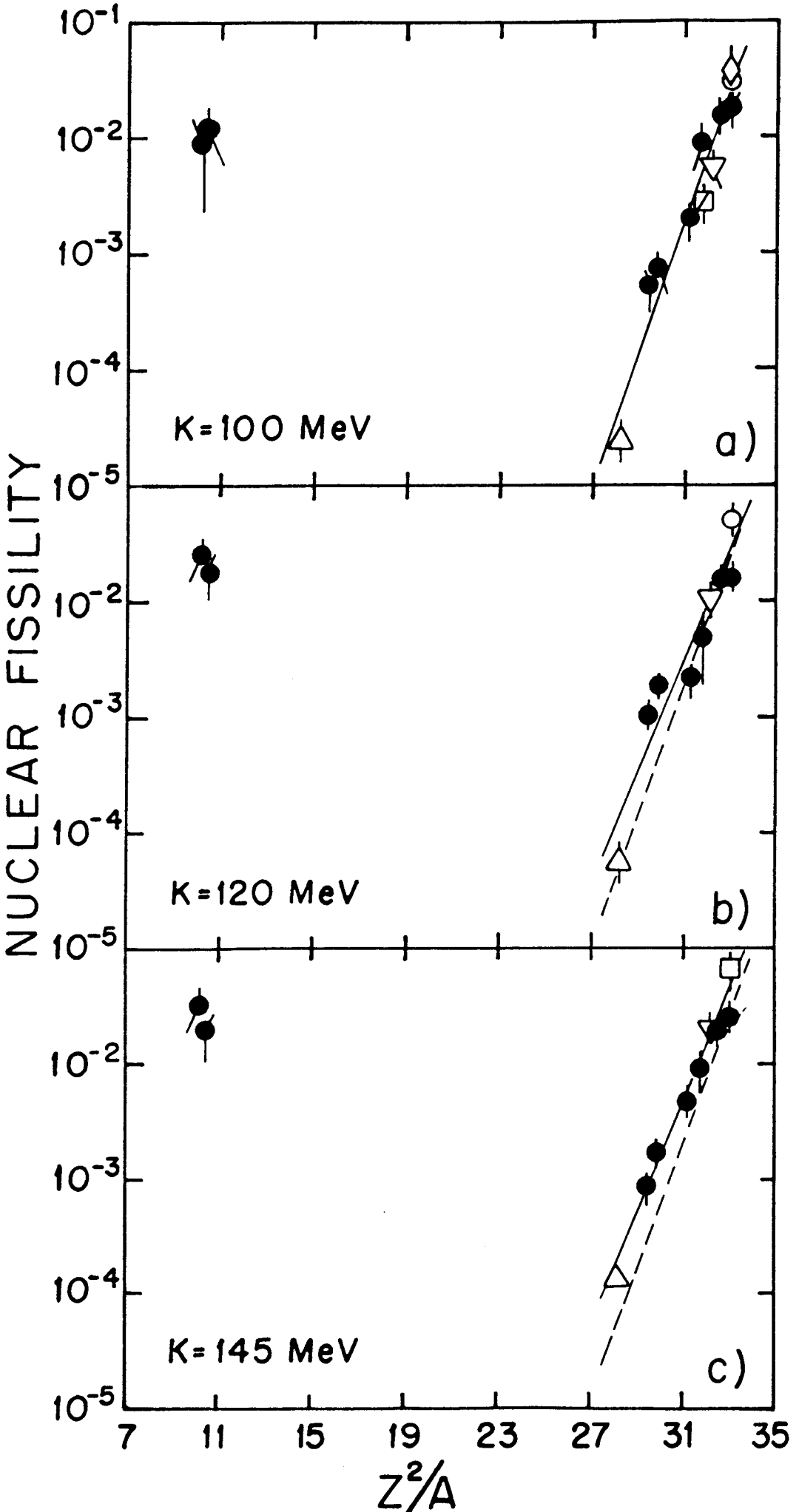
NUCLEAR FISSILITY
10^{-1}
10^{-2}
10^{-3}
10^{-4}
10^{-5}
K=100 MeV
a)
K=120 MeV
b)
K=145 MeV
c)
7
11
15
19
23
27
31
35
Z^2/A

Fig. 6